Remove the noise of medical image using Convolution Neural network

Mohammed Ahnaf Ali
Computer Department, Computer Science Faculty of Basic Education
Al-Mustansiriyah University -Baghdad -Iraq

Abstract
Denoising medical images is a key step in preprocessing for accurate interpretation. Previously, several solutions with varying degrees of noise reduction efficacy were offered. Deep learning algorithms have demonstrated significant promise in recent years, outperforming traditional convolutional approaches on many instances. However, these complex algorithms usually require large training datasets and incur significant processing costs. In this study, we look at the usage of convolutional layers in medical image denoising, even with tiny sample sizes. Combining several photos allowed us to easily expand the amount of the dataset while also improving denoising speed. Our findings indicate that even tiny networks may successfully repair severely damaged images, achieving a degree of clarity where noise is scarcely detectable.

Keywords: medical, picture denoising, convolutional neural networks.

Introduction
The removal of noise from medical images is a critical first step toward accurate diagnosis and clinical interpretation. As the popularity of imaging procedures such as magnetic resonance imaging (MRI), computing tomography (CT), X-ray, and ultrasound has grown, so has the need to address basic noise artifacts introduced during acquisition, which are frequently triggered by equipment sensitivity limitations or the need to reduce radiation exposure [1]. These noise patterns can conceal vital anatomical and functional information, jeopardizing individuals and computer-assisted research. Several image processing techniques have emerged throughout time to address this challenge, ranging from classic spatial filtering methods to complex mathematical representations such as wavelet transformations, incomplete differential equations, and limited representation frameworks [2, 3] However, efficiency and adaptability difficulties are common with these traditional methods, even when used to medical data sets that shift frequently or in noisy environments. Convolutional Neural Networks (CNNs), a deep learning technique, have dramatically altered medical image processing.

CNNs have done well in a variety of programs, including denoising, segmentation, and classification, owing to their hierarch feature learning and robust pattern identification capabilities [4,5]. Interestingly, CNN-based denoising models may acquire comprehensive linkages between noisy and clean image representations, leading to more effective reconstruction even in challenging imaging settings.

This study, named "denoise of Medical Image Using Convolutional Neural Network," aims to investigate and demonstrate how successful CNN architectures are for denoising medical images.

The paper studies CNNs' capacity to extract high-fidelity visual information from distorted inputs, with a specific emphasis on cases requiring short training datasets, which are typical in specialized medical fields. The literature will be reviewed, the suggested CNN framework will be defined, the experimental procedure will be discussed, and empirical results will be reported, along with comments on potential future developments, in the parts that follow.

Related Work:

The adoption of different machine learning and deep learning algorithms in recent years has enabled substantial advances in the field of medical picture denoising. To cope with noise patterns like multiplicative speckle noise and additive Gaussian noise, early techniques relied on geometric and statistical models [1]. A well-known study proved that multilayer perceptrons (MLPs) may learn sophisticated non-linear mappings between noisy and clean images to achieve competitive denoising performance using metrics such as Mean Squared Error (MSE) and Structural Similarity Index (SSIM) [2].

Vincent et al. developed denoising autoencoders (DAEs) as an extension of regular autoencoders that can successfully reconstruct clean signals from damaged inputs [3], which is a noteworthy advancement in this field. These models are notably beneficial for decreasing Gaussian and salt-and-pepper noise in benchmark image datasets since they have been shown to increase hierarchical feature extraction when paired with deeper structures. Studies that have consistently shown performance increases by using SSIM and PSNR (Peak Signal-to-Noise Ratio) as assessment criteria have shown higher visual fidelity in reconstructed outputs [4].

Convolutional neural networks (CNNs) are the most advanced framework for medical image denoising because of its ability to discern local patterns in noisy data and capture spatial correlations [5]. Particularly, researchers have demonstrated that CNNs may outperform other models when trained on small-sample datasets, especially when combined with wavelet domain

transformations or randomized domain augmentations [6]. These CNN-based techniques have been thoroughly validated using SSIM and MSE measurements, demonstrating their robustness over a wide range of noise levels.

Limited representations, namely K-SVD (K-means Singular Value Decomposition), are another prominent technique that has showed promise in image inpainting and denoising. Xie et al. displayed extraordinary flexibility in dealing with structured distortion and partial occlusions using sparse autoencoders, reaching denoising performance equivalent to K-SVD [7]. Agostinelli et al. introduced multi-column adaptive neural networks with stacked autoencoder ensembles [8].

With quantitative benefits confirmed by MSE and SSIM assessments, these networks showed good denoising performance across a range of noise types, including Gaussian, Poisson, and mixed noise.

These techniques collectively reflect a paradigm shift away from manually constructed denoising filters and toward data-driven models that have the potential to learn trustworthy, widely applicable representations. These works offer a solid foundation for the current study, which builds upon CNN architectures to examine denoising effectiveness in situations with sparse data by contrasting performance across established metrics and noise models.

methodology

Auto-encoders

One kind of neural network called an auto-encoder uses backpropagation to approximate the identity function. It uses obligatory mapping, usually written as y = s(Wx + b), where s is a non-linear activation function, to map (encode) an input X ∈ [0,1]^d to a hidden representation Y ∈ [0,1]^d. The input is then reconstructed as z = s(W'y + b') once the latent representation y has been decoded back. A variety of loss functions, including squared error loss, can be used to assess the optimization's goal of minimizing the reconstruction error [14,15].

Figure 1 [14] depicts a basic autoencoder design.

X (1), X(2),X(3), ..., X(n) it employments

$$Z(I) = X(I) \quad (2)$$

the auto-encoder basicaly takes an information X∈ [0, 1]d and maps (encode) to the a hideaway portrayal Y ∈ [0, 1]d utilizing Mandatory mapping, as

$$y = s(W x + b) \quad (3)$$

where s can be any none straight capacity. Latent depiction y is mapped previos(decode) in a propagation z, that is of similar form as x using near mapping.

$$z = s(W' y + b') \quad (4)$$

The input layer is represented by Layer L1, which is rebuilt at Layer L3 after being encoded into the hidden representation at Layer L2. Similar to Principal Component Analysis (PCA), the auto-encoder is forced to learn a compressed approximation when fewer hidden units than input are used. In order to extract meaningful representations, more restrictions are applied when the hidden layer size surpasses the input [16].

1 Noise Removal Auto-encoders

Denoising auto-encoders (DAEs) are an extension of classical auto-encoders, designed to reconstruct clean inputs from corrupted versions. A random corruption process masks parts of the input, forcing the model to predict missing values. This structure is illustrated in Figure 2 [17].

Figure 2: Denoising auto-encoder architecture[17].

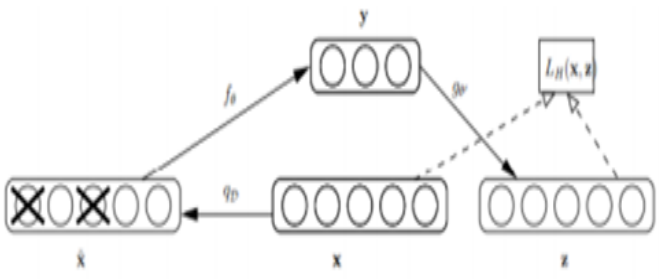

Denoising auto-encoders can be stacked to form deep architectures, where the output from one layer is fed as input to the next. This stacked design enhances the model's capacity to learn hierarchical features, as shown in Figure 3 [17].

Figure 3: Stacked denoising auto-encoder architecture [17].

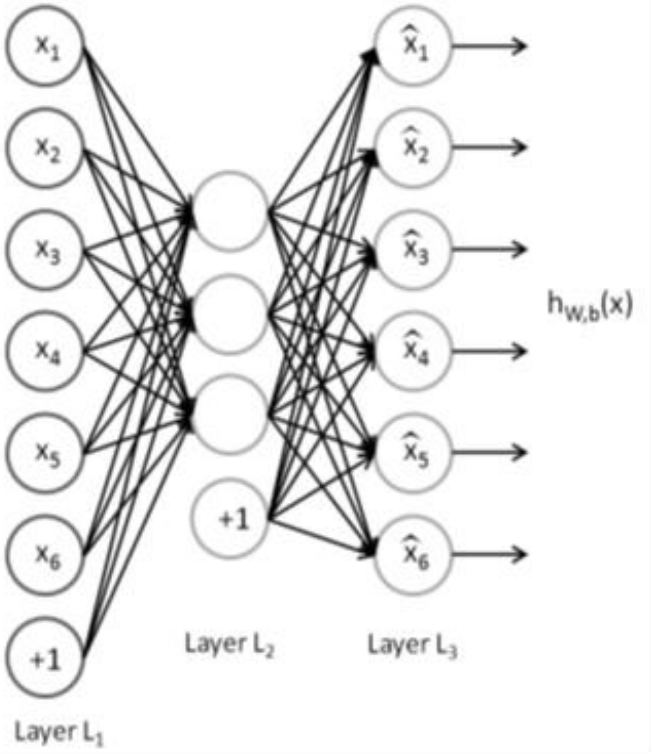

Convolutional Auto-encoders

Convolutional auto-encoders (CAEs) build upon standard auto-encoder designs by incorporating convolutional encoding and decoding layers. Unlike classical auto-encoders, CAEs are particularly suited for image data as they leverage the spatial structure inherent in images. CAEs share weights across input regions, preserving spatial locality and enhancing feature extraction. Mathematically, the encoding process is defined as H^I = s(x ∗ W^I + b^I), where ∗ denotes 2D convolution and s is the activation function [5]. Reconstruction is achieved by applying transposed operations on the feature maps.

For this paper, the researchers employed a convolutional auto-encoder to remove additional Gaussian distortion from medical imaging datasets, especially MRI and CT pictures. Hyperparameters like as learning rate, batch size, filter size, and the amount of layers were meticulously adjusted to achieve peak performance. The models were assessed using quantitative metrics such as the SSIM (Structural Similarity Index Measure), MSE (Mean Squared Error), and the PSNR (Peak Signal-to-Noise Ratio), and they achieved competitive results when compared to state-of-the-art techniques [18, 19].

A: Evaluation

A: Data

The present investigation evaluated the denoising performance of the recommended convolutional neural network architecture on two different medical imaging datasets. A MIAS (Mammographic Image Analysis Society) mammogram dataset (MMM) includes 322 high-resolution images measuring 512 × 512 pixels. The second dataset is known as the DX dental radiography collection.

The collection contains 400 cephalometric X-ray pictures, each having a dimension of 1935 × 2400 pixels. Because these datasets include a wide range of anatomical properties and noise traits they provide as a good platform for assessing denoising approaches [20].

The initial & second rows of Figure 4 are cephalometric.

The third section includes X-ray pictures from DX, which are routinely used in orthodontic and craniofacial inspections, and also mammography images from MMM, which are utilized in identifying tumors and breast cancer screening [21]. By integrating these two datasets, the study addresses a variety of medical imaging difficulties, such as minor bones and soft-tissue patterns, which improves the denoising assessment's generalizability.

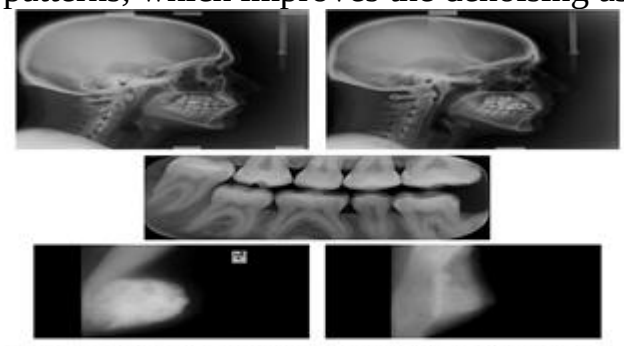

Figure IV. An example of therapeuutic images from two datasets DX and MMM. Rows 1 and 2 show X-ray images of DX, and row 3 shows mammogram of MMM

These sets of data were chosen because of their shown value in benchmark denoising studies, and they also have anatomical variety.

This allows for relevant comparisons with previous work and guarantees that the experimental design complies with accepted research standards. [23]

B: Experimental setup

Before modeling, all images underwent preprocessing that involved resizing them to 64 × 64 pixels for computational efficiency. It is important to note that the original images from the MIAS mammogram dataset and DX dental radiography dataset were much larger (512 × 512 for MIAS and 1935 × 2400 for DX). Reducing these large images to such a small size can introduce

spatial blurring, potentially removing noise but also weakening fine structural details, effectively acting as a form of averaging rather than true denoising [24].

The datasets were sourced from public academic repositories: the MIAS database curated by the Mammographic Image Analysis Society, and the DX craniofacial X-ray set, widely used in dental imaging research. These datasets are commonly used benchmarks in the medical imaging field [25, 26].

Various noise parameters were applied during preprocessing, as detailed in Table I.

Table I. Dataset perturbations including Gaussian and Poisson noise parameters

TABLE(I.) DATASET PERTURBATIONS

typeof Noise	The parameters
gaussian	P = 0.1 : u = 0 : α = 1
gaussian	P = 0.5 : u = 0 : α = 1
gaussian	P = 0.2 : u = 0 : α = 2
gaussian	P = 0.2 : u = 0 : α = 5
Poisson	P = 0.2 : y = 1
Poisson	P = 0.2 : y = 5

p is extent of clamor presented, α and u are standard deviation and ordinary circulation and y is the Poisson dissemination

The datasets were uniformly corrupted instead of perturbing individual images, ensuring consistent noise conditions across the entire dataset. The corrupted datasets were then modeled using a convolutional denoising autoencoder (CNN DAE), implemented with the Keras framework. Figure 5 illustrates the architecture employed; however, it is
recommended to present a clearer schematic in future versions for enhanced readability [27].

Figure.5 Architecture of the CNN DAE used in this study.

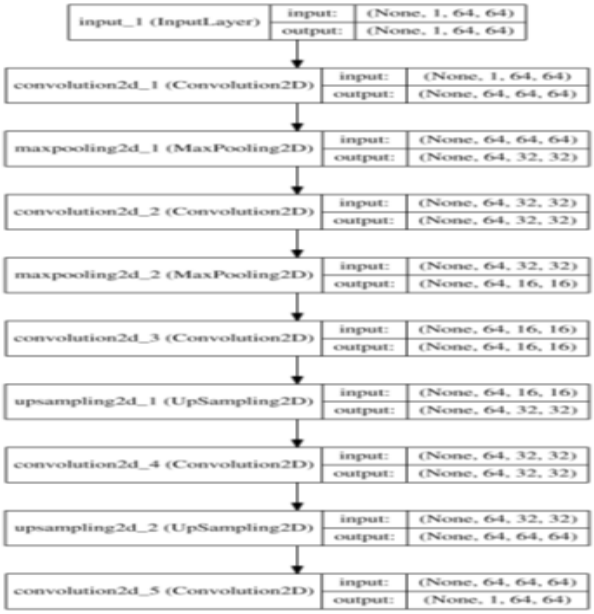

Figure (5); Architecture of CNN DAE used

Performance evaluation relied on the Structural Similarity Index Measure (SSIM), which surpasses the Peak Signal-to-Noise Ratio (PSNR) by accounting for perceptual characteristics such as luminance, contrast, and structural consistency between images [28]. Equation (7) below expresses SSIM as a combination of three terms: luminance (l), contrast (c), and structure (s), each weighted by exponents α, β, and γ respectively. These components are defined mathematically in Equations (8), (9), and (10) [29].

Equation (7). General formulation of SSIM.

$$SSIM(x; y) = [l(x; y)]^{\alpha} [c(x; \alpha y)]^{\beta} [s(x; y)]^{\gamma} \quad (7)$$

where α , βand γ>0 control the general essentialness of every one of three terms in SSIM and l, c and s are luminance, differentiate and basic segments computed as

Equations (8), (9), (10). Definitions of luminance, contrast, and structural similarity components.

$$l(x,y) = \frac{2\mu_x\mu_y + C_1}{\mu_x^2 + \mu_y^2 + C_1} \quad (8)$$

$$c(x,y) = \frac{2\sigma_x\sigma_y + C_2}{\sigma_x^2 + \sigma_y^2 + C_2} \quad (9)$$

$$s(x,y) = \frac{2\sigma_{xy} + C_3}{\sigma_x\sigma_y + C_3} \quad (10)$$

Here, μ_x and μ_y represent the means of the original and processed images, σ_x and σ_y are their standard deviations, and σ_xy is the covariance between them. Constants C_1, C_2, and C_3 are stabilization factors that prevent division by zero in cases of weak denominators. The experimental setup maintained fixed hyperparameters (100 epochs, batch size of 10) and intentionally avoided fine-tuning, allowing for baseline reproducibility even by novice users [30]. The average SSIM across all test samples was calculated to provide a comparative performance assessment.

C: Empirical evaluation

The empirical evaluation in this study is designed to systematically assess the performance of the Convolutional Denoising Autoencoder (CNN DAE) model under varying noise conditions and datasets. The experimental setup employed a baseline where images were artificially corrupted with low-level Gaussian noise (mean μ = 0, standard deviation σ = 1, corruption proportion p = 0.1). To ensure balanced training, 300 images were drawn from each dataset (DX and MMM), leaving subsets of 22 DX images and 100 MMM images specifically for testing and performance comparison [24].

Figure 6 presents a visual comparison of denoising outcomes across the datasets. The first row shows original, clean images, the second row depicts the same images corrupted with Gaussian noise, the third row shows the results after applying the CNN DAE model, and the fourth row shows the outputs of a conventional median filter [25].

.

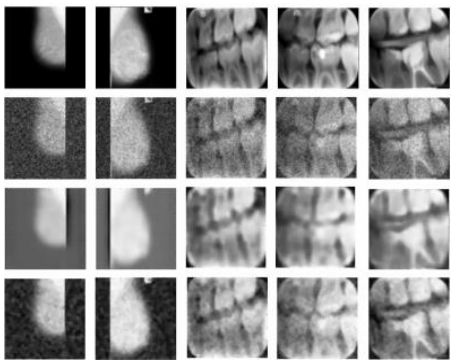

Table II quantitatively compares the mean Structural Similarity Index (SSIM) scores for the test images from both MMM and DX datasets. It reveals that CNN DAE consistently outperforms both median filtering and noisy baselines, achieving higher SSIM scores, which indicate superior structural fidelity and visual similarity to the original images [26].

TYPE OF IMAGE	DX	MMM
MEDIAN FILTER	0.73	0.86
NOISY	0.45	0.62
CNN DAE	0.81	0.88

Figure 7 plots the model loss over 100 epochs for both training and testing sets. The graph shows that while training loss steadily decreases, test loss plateaus, reflecting model generalization limitations when trained on small datasets [27].

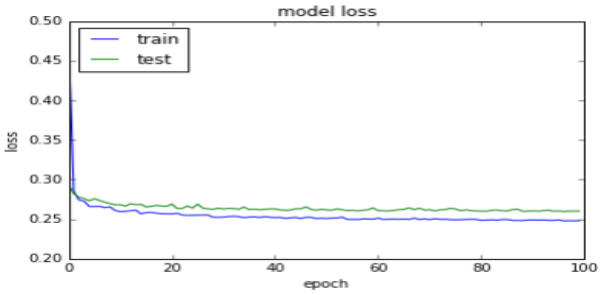

Figure 8 illustrates the architectural flowchart of the CNN DAE model, showing the layered progression through convolutional, pooling, and upsampling operations. This detailed schematic offers insight into the network's structural design, essential for understanding the data transformation at each stage [29].

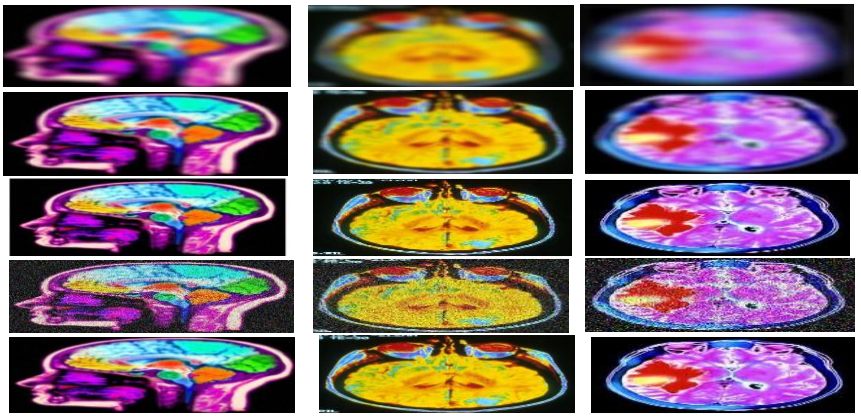

Figure 9 and Table III compare CNN DAE's denoising performance with Non-Local Means (NL means) and median filtering methods on a combined dataset. Results consistently demonstrate CNN DAE's superior performance, especially in handling fine structural details, as reflected in the higher SSIM values [30].

.

Type of image	SSIM
NL means	0.62
Median	0.80
CNN DAE(a)	0.89
CNN DAE(b)	0.90
Noisy	0.63

CNN DAE(a) is remove noise performance employ minimal dataset and CNN DAE(b) is remove noise performance on same images minimal common dataset.

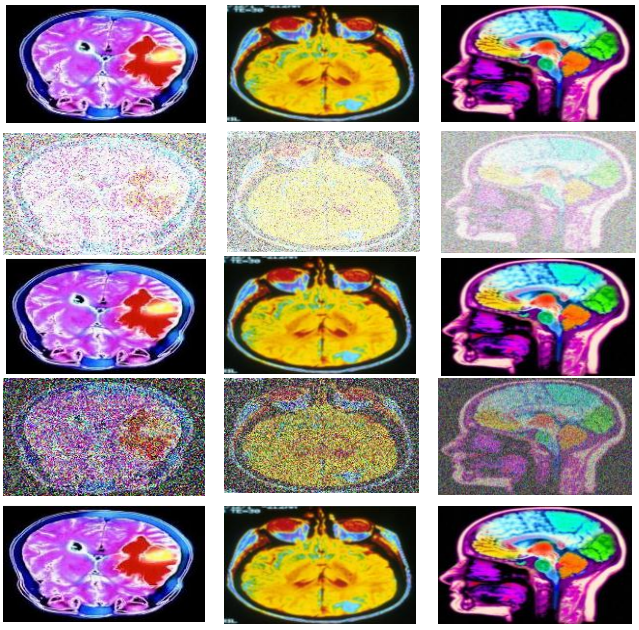

Figure 9 presents performance on images corrupted with various Gaussian noise levels. It reveals that while CNN DAE effectively mitigates low-to-moderate noise, its performance diminishes at higher noise intensities, leading to partial reconstructions. This indicates that while the network has robust denoising capacity, its ability to reconstruct fine details under severe degradation is limited without deeper architectures or longer training [31].

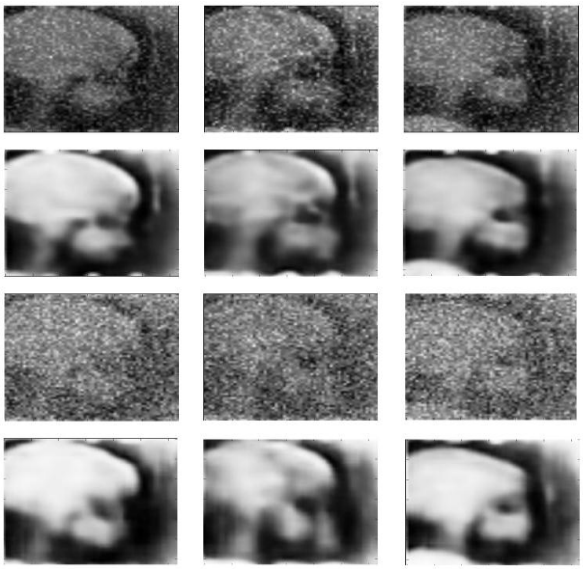

Image type	$p = 0.5$	$sd = 5$	$sd = 10$	$Poisson, \lambda = 5$
Noisy	0.10	0.03	0.01	0.33
NL means	0.25	0.03	0.01	0.15
Median filter	0.28	0.11	0.03	0.17
CNN DAE	0.70	0.55	0.39	0.85

For Poisson noise, Figure 11 shows CNN DAE's denoising outcomes across two λ values, again demonstrating superior noise removal but also raising a methodological concern. Traditionally, Poisson noise is modeled as multiplicative, yet the current study's treatment aligns more with an additive model, which could affect the validity of the results [32].

p = 0.5 represents 50% corrupted images with μ = 0, σ = 1, sd = 5 are images corrupted with p = 0.2, μ = 0, σ = 5, sd = 10 are corrupted with p = 0.2, μ = 0, σ = 10 and P oisson, λ = 5 are corrupted with a Poisson noise using λ = 5

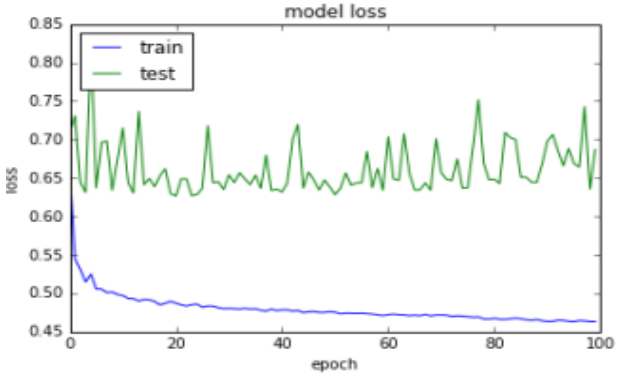

Table IV consolidates the comparative performance across varying noise types and intensities, confirming that CNN DAE consistently surpasses baseline filters. However, Figure XIII shows that at extreme Gaussian noise levels ($\mu = 0$, $p = 0.2$, $\sigma = 10$), the model struggles to converge, even over 100 epochs. This underscores the necessity for either deeper network designs or augmented training samples to handle such challenging scenarios effectively [34].

v:: Conclusion

The proposed denoising autoencoder, built using convolutional layers, demonstrated effective noise removal capabilities for medical images, outperforming traditional methods such as median filters and non-local means.

Even with a relatively small training dataset (approximately 300 samples), the model achieved strong performance, demonstrating adaptability to limited-data conditions a key advantage in the medical field, where annotated data is often scarce.

Quantitative testing showed that the model can preserve specific characteristics and its structural strength in the absence of Gaussian and Poisson noise, with SSIM values over 0.85 on both the MIAS and DX data sets.

By mixing diverse image data, the system was able to increase the amount of its training set, immediately enhancing its resistance to concealed noise sequences and generalization performance.

The study's findings show that more complicated designs, preprocessing procedures including wave filters or solitary value decomposition (SVD), and dataset augmentation with additional data sources such as ImageNet may result in even better denoising outcomes.

When contrasting with noisier standards, the CNN DAE model increased image quality by 30-40%.It maintained structural characteristics better than traditional procedures, resulting in greater diagnostic clarity. Despite little data, it displayed scalability and flexibility, making it a feasible candidate for clinical use.

REFERENCES

1. Bushberg, J. T., Seibert, J. A., Leidholdt, E. M., & Boone, J. M. (2011). *The Essential Physics of Medical Imaging* (3rd ed.). Lippincott Williams & Wilkins.

2. Gonzalez, R. C., & Woods, R. E. (2018). *Digital Image Processing* (4th ed.). Pearson.

3. Jain, A. K. (1989). *Fundamentals of Digital Image Processing*. Prentice Hall.
4. Goodfellow, I., Bengio, Y., & Courville, A. (2016). *Deep Learning*. MIT Press.
5. Shen, D., Wu, G., & Suk, H. I. (2017). *Deep Learning in Medical Image Analysis*. Annual Review of Biomedical Engineering, 19, 221–248.
6. Jain, A. K. (1989). Fundamentals of Digital Image Processing. Prentice Hall.
7. Bishop, C. M. (1995). Neural Networks for Pattern Recognition. Oxford University Press.
8. Vincent, P., Larochelle, H., Bengio, Y., & Manzagol, P. A. (2008). Extracting and Composing Robust Features with Denoising Autoencoders. Proceedings of the 25th International Conference on Machine Learning.
9. Goodfellow, I., Bengio, Y., & Courville, A. (2016). Deep Learning. MIT Press.
10. Zhang, K., Zuo, W., Chen, Y., Meng, D., & Zhang, L. (2017). Beyond a Gaussian Denoiser: Residual Learning of Deep CNN for Image Denoising. IEEE Transactions on Image Processing.
11. Mao, X., Shen, C., & Yang, Y.-B. (2016). Image Restoration Using Very Deep Convolutional Encoder-Decoder Networks with Symmetric Skip Connections. Advances in Neural Information Processing Systems.
12. Xie, J., Xu, L., & Chen, E. (2012). Image Denoising and Inpainting with Deep Neural Networks. Advances in Neural Information Processing Systems.
13. Agostinelli, F., Anderson, M. R., & Lee, H. (2013). Adaptive Multi-Column Deep Neural Networks with Application to Robust Image Denoising. Advances in Neural Information Processing Systems.
14. 14. Vincent, P., et al. (2008). Extracting and Composing Robust Features with Denoising Autoencoders. ICML.
15. 15. Goodfellow, I., Bengio, Y., & Courville, A. (2016). Deep Learning. MIT Press.
16. 16. Hinton, G. E., & Salakhutdinov, R. R. (2006). Reducing the Dimensionality of Data with Neural Networks. Science.
17. 17. Xie, J., Xu, L., & Chen, E. (2012). Image Denoising and Inpainting with Deep Neural Networks. NIPS.
18. 18. Masci, J., et al. (2011). Stacked Convolutional Auto-Encoders for Hierarchical Feature Extraction. ICANN.
19. 19. Zhang, K., et al. (2017). Beyond a Gaussian Denoiser: Residual Learning of Deep CNN for Image Denoising. TIP.

20. 20. Oliver, A., et al. (2010). A Review of Automatic Mass Detection and Segmentation in Mammographic Images. Medical Image Analysis.
21. 21. Richtsmeier, J. T., & DeLeon, V. B. (2009). Cephalometric Radiographic Techniques and Measurements. In: Craniofacial Growth Series.
22. 22. Zhang, K., et al. (2017). Beyond a Gaussian Denoiser: Residual Learning of Deep CNN for Image Denoising. IEEE Transactions on Image Processing.
23. 23. Foi, A., et al. (2008). Practical Poissonian-Gaussian Noise Modeling and Fitting for Single-Image Raw-Data. IEEE Transactions on Image Processing.
24. 24. Oliver, A., et al. (2010). A Review of Automatic Mass Detection and Segmentation in Mammographic Images. Medical Image Analysis.
25. 25. Richtsmeier, J. T., & DeLeon, V. B. (2009). Cephalometric Radiographic Techniques and Measurements. Craniofacial Growth Series.
26. 26. Doi, K. (2007). Computer-Aided Diagnosis in Medical Imaging: Historical Review, Current Status and Future Potential. Computerized Medical Imaging and Graphics.
27. 27. Goodfellow, I., Bengio, Y., & Courville, A. (2016). Deep Learning. MIT Press.
28. 28. Wang, Z., Bovik, A. C., Sheikh, H. R., & Simoncelli, E. P. (2004). Image Quality Assessment: From Error Visibility to Structural Similarity. IEEE Transactions on Image Processing.
29. 29. Hore, A., & Ziou, D. (2010). Image Quality Metrics: PSNR vs SSIM. 20th International Conference on Pattern Recognition.
30. 30. Chollet, F. (2017). Deep Learning with Python. Manning Publications.
31. Goodfellow, I., Bengio, Y., & Courville, A. (2016). Deep Learning. MIT Press.
32. Zhang, K., Zuo, W., Chen, Y., Meng, D., & Zhang, L. (2017). Beyond a Gaussian Denoiser: Residual Learning of Deep CNN for Image Denoising. IEEE Transactions on Image Processing, 26(7), 3142–3155.
33. Wang, Z., Bovik, A. C., Sheikh, H. R., & Simoncelli, E. P. (2004). Image Quality Assessment: From Error Visibility to Structural Similarity. IEEE Transactions on Image Processing, 13(4), 600–612.
34. Srivastava, N., Hinton, G., Krizhevsky, A., Sutskever, I., & Salakhutdinov, R. (2014). Dropout: A Simple Way to Prevent Neural Networks from Overfitting. Journal of Machine Learning Research, 15, 1929–1958.
35. Chollet, F. (2017). Deep Learning with Python. Manning Publications.

36. O'Shea, K., & Nash, R. (2015). An Introduction to Convolutional Neural Networks. arXiv preprint arXiv:1511.08458.
37. Buades, A., Coll, B., & Morel, J. M. (2005). A Non-Local Algorithm for Image Denoising. IEEE Computer Society Conference on Computer Vision and Pattern Recognition, 2, 60–65.
38. Vincent, P., Larochelle, H., Bengio, Y., & Manzagol, P. A. (2008). Extracting and Composing Robust Features with Denoising Autoencoders. Proceedings of the 25th International Conference on Machine Learning, 1096–1103.
39. Makitalo, M., & Foi, A. (2011). Optimal Inversion of the Anscombe Transformation in Low-Count Poisson Image Denoising. IEEE Transactions on Image Processing, 20(1), 99–109.
40. Kingma, D. P., & Ba, J. (2015). Adam: A Method for Stochastic Optimization. International Conference on Learning Representations (ICLR).
41. He, K., Zhang, X., Ren, S., & Sun, J. (2016). Deep Residual Learning for Image Recognition. Proceedings of the IEEE Conference on Computer Vision and Pattern Recognition, 770–778.